Acta Crystallographica Section D
Biological Crystallography
ISSN 0907-4449

Structures of cyanide, nitric oxide and hydroxylamine complexes of *Arthromyces ramosus* peroxidase at 100 K refined to 1.3 Å resolution: coordination geometries of the ligands to the haem iron

Keiichi Fukuyama* and Toshihiro Okada

Department of Biological Sciences, Graduate School of Science, Osaka University, Toyonaka, Osaka 560-0043, Japan

Correspondence e-mail: fukuyama@bio.sci.osaka-u.ac.jp

Received 22 November 2006
Accepted 24 January 2007

PDB References: CN-bound form of *Arthromyces ramosus* peroxidase, 2e39, r2e39sf; NO-bound form, 2e3a, r2e3asf; HA-bound form, 2e3b, r2e3bsf.

1.3 Å resolution crystal structures of the cyanide, nitric oxide and hydroxylamine complexes of *Arthromyces ramosus* peroxidase (ARP), a class II peroxidase belonging to the plant peroxidase superfamily, have been determined. Anisotropic temperature factors were introduced for all non-H atoms of these complexes using *SHELX*-97 and stereochemical constraints were applied to the protein, protoporphyrin and sugar moieties, but not to the coordination geometries to the haem iron. These refinements identified multiple conformations for several side chains and revised the side-chain conformations of several residues. Little difference was observed in the structures of the polypeptides, haem and sugar moieties and in the coordinations to two calcium ions in these complexes. Characteristic coordination geometries of each ligand to the haem iron were observed. CN^- binds to the haem iron in a tilt mode (Fe···C—N = 170°), whereas NO and hydroxylamine bind in bent modes (Fe···N—O = 125° and Fe···NH_2—OH = 111°). CN^- is directed toward the distal histidine (His56) and forms a hydrogen bond with the N^{ε} atom, whereas NO and hydroxylamine are directed away from His56. The Fe atoms of ARP–CN and ARP–NO, in which the haem irons are both in low-spin states, are approximately in the pyrrole N plane, whereas the iron in native ARP, which is in a five-coordinated high-spin state, deviates markedly from the plane.

1. Introduction

Haem peroxidases are enzymes that catalyze the oxidation of various organic and inorganic compounds using H_2O_2 or organic peroxides. These enzymes have broad substrate specificity and various biological functions (Smith & Veitch, 1998). For example, ascorbate peroxidase, a class I peroxidase belonging to the plant peroxidase superfamily (Welinder, 1992), is involved in H_2O_2 scavenging using ascorbate as a reducing substrate (Chen & Asada, 1989), while the major function of horseradish peroxidase (HRP), a class III peroxidase, is to oxidize small aromatic molecules, thereby cross-linking them to produce the plant cell wall (Gajhede, 2001). The peroxidase from the fungus *Arthromyces ramosus* (ARP), a class II peroxidase, is found in the extracellular medium (Shinmen *et al.*, 1986). ARP and other class II peroxidases, such as lignin peroxidase and *Phanerochaete chryosporium* manganese peroxidase, are secreted enzymes (Fukuyama, 2001). ARP produces high levels of chemiluminescence when the substrate luminol is oxidized and thus has potential analytical uses in the accurate determination of biological substances (Akimoto *et al.*, 1990).

Following translation, a signal peptide at the N-terminus of the nascent ARP is cleaved, producing a polypeptide of 344 amino-acid residues in which the N-terminal residue is pyroglutamate (Sawai-Hatanaka *et al.*, 1995). The mature ARP contains one haem group and two calcium ions and has carbohydrates attached to the Asn143 and Ser339 residues. The structure of ARP (Fig. 1) determined by crystallographic analysis at 1.9 Å resolution (Kunishima *et al.*, 1994) is similar to the structures of cytochrome *c*, the ascorbate peroxidases of class I (Finzel *et al.*, 1984; Sharp *et al.*, 2003), the peanut, horseradish and barley peroxidases of class III (Schuller *et al.*, 1996; Gajhede *et al.*, 1997; Henriksen *et al.*, 1998) and other class II peroxidases (Poulos *et al.*, 1993; Sundaramoorthy *et al.*, 1994). Characteristic features of ARP include the presence of two Ca^{2+}-binding sites, a wide entrance to the tunnel leading to the active site and an additional peptide segment at the C-terminus.

As for other haem enzymes, the substrates of the haem peroxidases bind to the distal sides of the haem to be activated and processed. The manner of ligand binding to the haem iron is of fundamental significance in understanding the chemical properties of haem enzymes. For example, the coordination geometries of the haem ligands correlate to enzyme function in haem oxygenase, an enzyme that catalyzes the cleavage of haem at the *α-meso* carbon using O_2 and reducing equivalents to produce biliverdin IXα, CO and iron; discrimination between O_2 (substrate) and CO (product) is achieved, at least in part, by differences in their coordination modes to the haem iron and the enzyme thus escapes product inhibition (Sugishima *et al.*, 2003). Defining the orientation of the diatom ligand requires high-resolution analysis, but ligand-binding modes determined by high-resolution X-ray data are rather rare. Imposing restraints on structure refinements may lead to uncertainty in the mode of ligand binding or in some cases to biased results (Stec & Phillips, 2001).

The use of high-intensity and well collimated X-rays from synchrotron-radiation sources and cryogenic techniques for protein crystals have enabled significant improvements in the resolution of diffraction data, in some cases to atomic resolution. Diffraction data at atomic resolution permit structural refinement without restraints and allow the introduction of anisotropic temperature factors, which produce detailed models that can show such features as multiple conformations of residues, discrimination of atomic species and, in some cases, the location of H atoms (Dauter *et al.*, 1997; Longhi *et al.*, 1998). The number of protein structures determined at atomic resolution has significantly increased and the analysis has recently been extended to medium-size proteins (Tame *et al.*, 1996; Ermler *et al.*, 1997; Matsumoto *et al.*, 1999; Tame, 2000; Shimizu, Nakatsu *et al.*, 2002; Shimizu, Park *et al.*, 2002). The structures of the CN^- and hydroxylamine (HA) complexes of ARP at room temperature have been determined at 1.6 and 2.0 Å resolution, respectively (Fukuyama *et al.*, 1995; Wariishi *et al.*, 2000); a more accurate determination of the binding geometries of the ligands to the haem iron has been awaited.

We have determined the crystal structures of the NO complex of ARP in addition to the CN^- and HA complexes at 100 K using diffraction data to 1.3 Å resolution. Here, we report the characteristic binding modes of these ligands to the ARP haem iron. In addition, we describe the side-chain conformations that were revised or identified by this analysis.

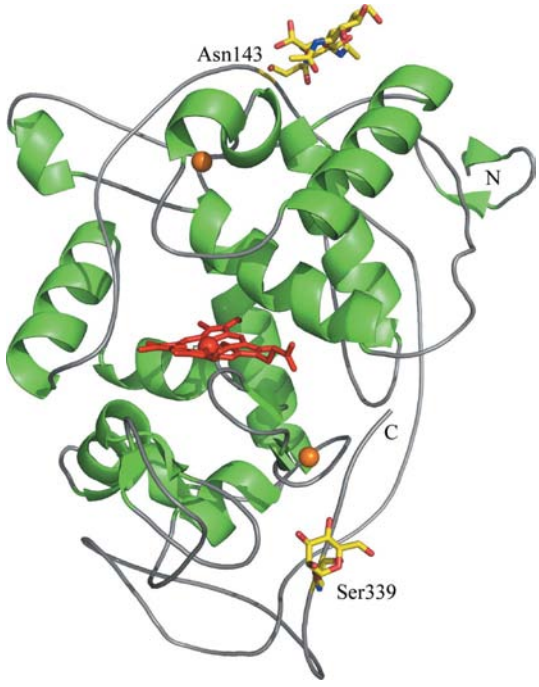

Figure 1
Schematic representation of ARP. The haem group is shown in red and calcium ions in orange. The carbohydrates are shown as stick models, in which C, N and O atoms are in yellow, blue and red, respectively. This figure was prepared with the program *PyMOL* (DeLano, 2002).

2. Materials and methods

2.1. Preparation of crystals of ARP complexes

ARP was purified and crystallized as previously described (Kunishima *et al.*, 1993). Because the haem iron of ARP binds ammonia derived from the ammonium sulfate used as precipitant above neutral pH (Kunishima *et al.*, 1996), ARP crystals were soaked in 50 m*M* sodium acetate buffer pH 5.6 containing 37% saturated ammonium sulfate for 2 h prior to use. Ligand-free crystals were then soaked for a few hours in a buffer containing each ligand. The concentrations of KCN and hydroxylamine were 2 and 50 m*M*, respectively. An NO-containing solution was prepared by adding a small amount of NOC-12, an autocatalytic donor (Dojindo), to the buffer; the exact concentration of NO was unknown. Conversion to the ligand-bound form appeared to be complete in a few minutes, as assessed by visual monitoring of the colour change of the crystal.

2.2. X-ray data collection

The crystals were flash-cooled to 100 K without transfer to a cryoprotectant solution. This procedure improved the maximum resolution of the diffraction but produced ice

Table 1
Results of data collection and structural refinement.

Values in parentheses are for the highest resolution shell.

Data set	ARP–CN	ARP–NO	ARP–HA
Data collection			
Unit-cell parameters (Å)	a = 73.84, c = 115.7	a = 73.77, c = 115.8	a = 73.15, c = 114.9
Oscillation angles (°)	1.0/3.0	0.8/3.0	0.8/2.4
Resolution range (Å)	20–1.3 (1.34–1.30)	20–1.3 (1.37–1.30)	20–1.3 (1.37–1.30)
No. of measurements	697137	610551	629860
No. of unique reflections	78519	78918	78980
Completeness (%)	99.3 (97.1)	98.3 (92.9)	99.4 (97.4)
$R_{\rm merge}$† (%)	6.6 (23.6)	6.6 (26.4)	6.8 (27.9)
Structural refinement			
Resolution range (Å)	20–1.3	10–1.3	12–1.3
$R_{\rm cryst}/R_{\rm free}$‡	15.0/20.3	14.8/20.1	14.1/19.9
No. of water molecules	387	403	425
R.m.s. deviations from ideality			
Bond lengths (Å)	0.011	0.011	0.012
Bond angles (°)	2.1	2.2	2.2
Ramachandran plot			
Most favoured regions (%)	91.6	91.3	90.2
Additional allowed regions (%)	8.4	8.7	9.8
Average temperature factors (Å^2)			
Main chain	13.0	13.4	11.8
Side chain	15.0	15.2	13.4
Haem group	8.9	9.2	7.9
Distal ligand	10.7	14.1	15.2
Water molecules	21.1	21.7	20.3

† $R_{\rm merge} = \sum_{hkl}\sum_i |I_i(hkl) - \langle I(hkl)\rangle| / \sum_{hkl}\sum_i I_i(hkl)$. ‡ $R_{\rm free}$ was calculated for 5% of reflections randomly excluded from the refinement.

crystals, which gave several strong spots on each frame. All cryoprotectant solutions that we tried reduced the diffraction quality. Diffraction data were collected at λ = 0.71 Å by the oscillation method at 100 K on a MAR CCD detector in BL41XU at SPring-8. The crystals were tetragonal, belonging to space group $P4_22_12$, and contained one ARP molecule per asymmetric unit. Two data sets were collected for each crystal in order to increase the coverage of the dynamic range of the intensities: the first data set was collected with a small oscillation angle and an intense X-ray beam and the second data set was collected with a wide oscillation angle and an attenuated X-ray beam. Diffraction images were processed with *MOSFLM* (Leslie, 1992) and the intensities were scaled with *SCALA* in *CCP*4 (Collaborative Computational Project, Number 4, 1994). The maximum resolutions collected were 1.3 Å. Results of data collection are given in Table 1.

2.3. Structure refinement

The initial model for ARP–CN was the native ARP structure at room temperature refined at 1.8 Å resolution (Kunishima *et al.*, 1996), from which solvent molecules were excluded. This model was refined using the diffraction data reported here by alternate application of model revision/water location against $(2F_o - F_c)$ and $(F_o - F_c)$ maps and simulated annealing using the program *X-PLOR* (Brünger, 1992). Resolution was extended stepwise to 1.5 Å. Subsequently, anisotropic temperature factors were introduced using the diffraction data to 1.3 Å resolution and the conjugate gradient least-squares method with *SHELX*-97 (Sheldrick & Schneider, 1997), in which default values were used for the distance, planarity, chiral volume and antibumping restraints. Multiple conformations for some side chains were taken into account. At the final stage of refinement, the ligand was fitted into the density of the $(F_o - F_c)$ and $(2F_o - F_c)$ maps and included in the refinement, where the bond length in the ligand was fixed to the established value but neither the Fe···C distance nor the Fe···C—N angle was restrained. H atoms were also included in the refinement at riding positions. The crystal structures of the other complexes were refined in a similar way. The refinement statistics are given in Table 1.

3. Results and discussion

3.1. Quality and improvement of the model

The crystallographic measurements at 100 K using synchrotron radiation reported here yielded intensity data to 1.3 Å resolution for the crystals of the three complexes. In addition to providing the first data collection for ARP–NO, these data collections have increased the numbers of reflections for ARP–CN and ARP–HA by 2.1-fold and 3.6-fold, respectively, compared with those obtained previously at room temperature (Fukuyama *et al.*, 1995; Wariishi *et al.*, 2000). The new data have allowed refinement with anisotropic temperature factors that impose no restraints on the coordination geometries of the ligands. In addition, these analyses located as many as twice the number of water molecules as located by previous data sets. The final $R/R_{\rm free}$ values for ARP–CN, ARP–NO and ARP–HA are 15.0/20.3, 14.8/20.1 and 14.1/19.9, respectively. The standard uncertainties for Fe and the average of C, N and O atoms of each complex were 0.006 and 0.06 Å, respectively, from inversion of the full-matrix least squares in *SHELX*-97.

The resulting electron-density maps showed that the flipped orientation of the haem group is absent from all three

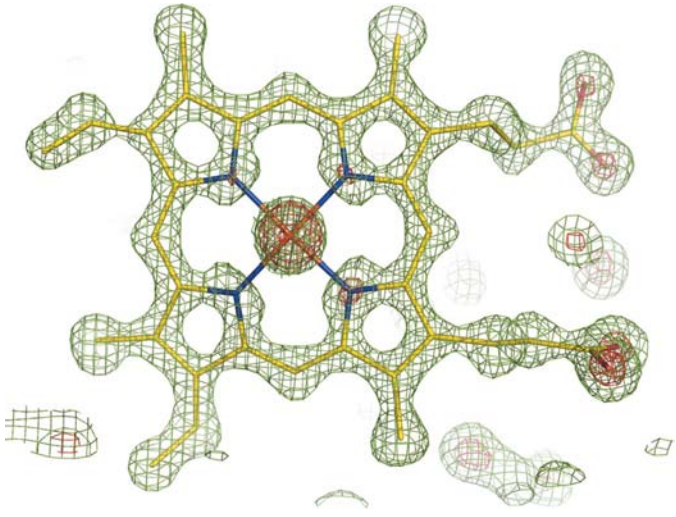

Figure 2
Electron-density map $(2F_o - F_c)$ for the haem of ARP–CN at 1.3 Å resolution. Contour levels: green, 2σ, red, 6σ.

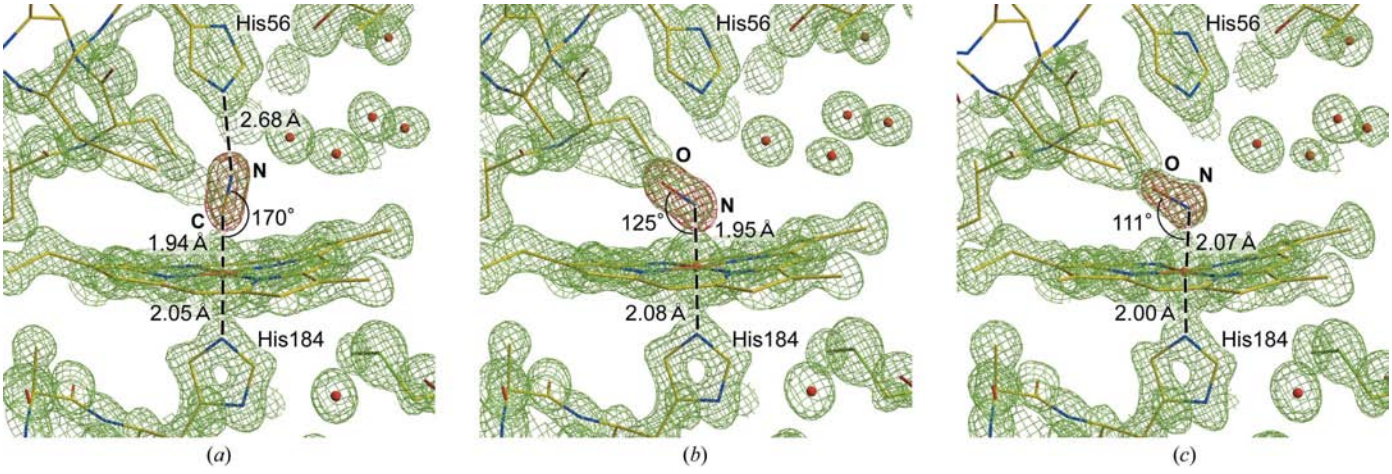

Figure 3
Electron density near the haem iron. (*a*) ARP–CN, (*b*) ARP–NO, (*c*) ARP–HA. The final models are superimposed on the maps. Green, $(2F_o - F_c)$ map (2σ); red, OMIT $(F_o - F_c)$ map (6σ). The geometries of ligand binding to the haem iron are shown, where the distances and angles are given in Å and degrees, respectively.

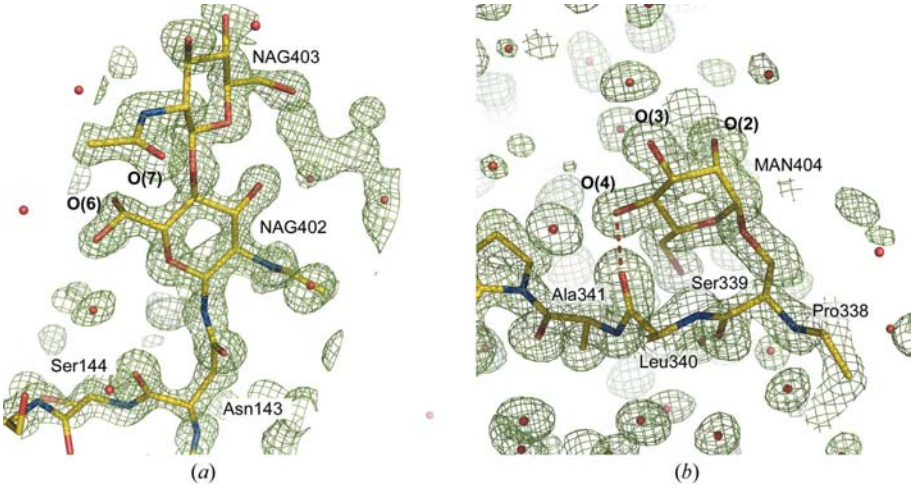

Figure 4
Conformations of sugar moieties. (*a*) Two *N*-acetylglucosamine residues bound to Asn143 and (*b*) mannose residue bound to Ser339. The stick models are superimposed on the $(2F_o - F_c)$ map contoured at the 1.5σ level.

complexes (Fig. 2); this contrasts with cytochrome P450 (Shimizu, Park *et al.*, 2002) and haem oxygenase in complex with haem (Sugishima *et al.*, 2002). The main-chain atoms of the three complexes are superimposable with an r.m.s. deviation of less than 0.23 Å. When the side-chain atoms, haem group, Ca^{2+} ions and carbohydrate moieties are included in the superimposition, the r.m.s. deviations are less than 0.35 Å, indicating that, except for the ligand-binding modes, the structures of the complexes are substantially identical to each other.

3.2. Coordination geometries of the ligands

The detailed structures of the three complexes around the haem iron are shown in Fig. 3. The coordination geometries of the distal and proximal ligands to the haem iron in each complex are listed in Table 2. CN^- binds to the haem iron in tilt mode (Fe···CN distance = 1.94 Å, Fe···CN angle = 170°). A similar manner of CN^- binding was observed in the HRP–CN–ferulic acid complex (Henriksen *et al.*, 1999) and the cyanide complex of ascorbate peroxidase (Badyal *et al.*, 2006); the crystal structures of these two complexes have been determined at 1.4 Å resolution, showing Fe···CN angles of 159 and 163°, respectively. In ARP–CN, the distance between the N atom of the CN and the N^{ε} of His56 is 2.68 Å, indicating that these atoms are hydrogen bonded. Hydrogen bonds were also observed between the cyanide ligand and the N^{ε} atom of the distal histidine in the HRP–CN–ferulic acid and cyanide–ascorbate peroxidase complexes. The existence of a hydrogen bond was also indicated in the cyanide complex of lignin peroxidase by NMR spectroscopy (de Ropp *et al.*, 1991), indicating that hydrogen bonding may commonly occur upon cyanide binding in members of the plant peroxidase superfamily.

Unlike cyanide, NO binds to the haem iron of ARP in the bent mode (Fe···NO distance = 1.95 Å, Fe···N—O angle = 125°). In ARP–NO, the ligand is directed away from His56 and it does not appear that there is a direct interaction between NO and the protein moiety at pH 5.5. A 1.25 Å resolution structure of NO bound to the W41A mutant of ascorbate peroxidase showed that NO binds to the haem iron in the bent mode but adopts two conformations (Badyal *et al.*, 2006). However, in contrast to the case of ARP–NO, the NO ligand in either conformation forms a hydrogen bond to the N^{ε} atom of the distal histidine in the W41A ascorbate peroxidase mutant.

It has been reported previously that HA binds to the ARP haem iron and inhibits compound I formation in a competitive

Table 2
Coordination geometries of the ligands of the haem iron.

Data set	ARP–CN	ARP–NO	ARP–HA
Distances (Å)			
Fe···*X*†	1.94 (3)	1.95 (3)	2.07 (3)
His56 N^{ε}···*Y*†	2.68 (3)	3.25 (4)	3.31 (4)
Fe to pyrrole N plane‡	0.05 (1)	0.03 (1)	0.11 (1)
Fe···His184 N^{ε}	2.05 (2)	2.08 (2)	2.00 (2)
Angles (°)			
Fe···*X*—*Y*	170 (3)	125 (3)	111 (2)
His184 N^{ε}···Fe···*X*†	174.9 (9)	177.2 (8)	175.1 (9)

† *X* and *Y* are the two non-H atoms of each ligand, where *X* is the atom that is coordinated to the haem iron. ‡ The pyrrole N plane was calculated using the coordinates of the four pyrrole N atoms (N_A, N_B, N_C and N_D).

manner (Wariishi *et al.*, 2000). It has also been shown that the dissociation constant of HA is pH-dependent and that HA binds to the haem iron through its N atom. The high-resolution structural analysis of ARP–HA shows that the HA ligand binds to the haem iron in a manner similar to NO, but with a greater tilt (Fe···N distance = 2.07 Å, Fe···N—O angle = 111°). In ARP–HA, HA is directed away from His56; the distance between the OH group of HA and the N^{ε} atom of His56 is 3.31 Å. Therefore, the existence of a hydrogen bond between HA and His56 suggested by a previous 2 Å resolution analysis of ARP–HA (Wariishi *et al.*, 2000) is not correct: owing to relatively low-resolution density in the previous 2 Å analysis at room temperature, the orientation of HA was assigned incorrectly. Although the crystal structure of the enzyme involved in HA oxidation has been reported (Igarashi *et al.*, 1997), no structural study has been undertaken to determine the binding mode of HA to the haem iron. In light of the significance of HA to the enzymatic activity, the binding mode of HA to the haem iron and the properties of the interaction between HA and the haem iron must be further characterized by spectroscopy as well as by X-ray analysis.

The Fe atoms in the three complexes are all in six-coordinated low-spin states and lie approximately in the haem plane. This is in marked contrast to the native (ligand-free) ARP, which contains an Fe atom that is in a five-coordinated high-spin state (Kunishima *et al.*, 1996) and deviates markedly from the haem plane toward the proximal side[1].

3.3. Structures of side chains and carbohydrates

The electron-density maps at 1.3 Å resolution unambiguously defined the side-chain conformations; the torsion angles of the $C^{\alpha}—C^{\beta}$ and $C^{\beta}—C^{\gamma}$ bonds for several Leu residues and the $C^{\alpha}—C^{\beta}$ bonds of a few Val and Thr residues were corrected (data not shown). In addition, it was found that the imidazole ring of His110 should be rotated around the $C^{\beta}—C^{\gamma}$ bond. Refinement with the revised conformation yielded reasonable temperature factors for the atoms comprising the imidazole ring as well as favourable geometry for the hydrogen bond between His110 and the neighbouring residue. The analyses also enabled us to identify multiple conformations for the side chains of Val29, Val47, Asn85, Ser132, Asp165, Val268 and Val308.

The conformation of the mannose residue bonded to Ser339 was clearly visible (Fig. 4*b*). The O^{γ} (Ser339) and O(2) atoms occupy axial positions of the chair-form ring. The O(4) atom of the mannose residue is hydrogen bonded to the main-chain O atom of Leu340. It was found that O(6) of *N*-acetylglucosamine 402 occupies two sites (Fig. 4*a*). All of the hydroxy, *N*-acetyl and hydroxymethyl groups of the two sugar residues (NAG402 and NAG403) as well as the bonds linking the two sugar chains occupy equatorial positions. In the crystal, the two sugar residues lie parallel to the corresponding sugar residues related by the crystallographic twofold axis. In addition to an intramolecular hydrogen bond between O(7) of NAG403 and Arg104 $N^{\eta 1}$, an intermolecular hydrogen bond between O(7) of NAG402 and Asn143 N^{δ} may contribute to fixing the conformations of the sugar moieties. The carbohydrate beyond the first two *N*-acetylglucosamine residues bonded to Asn143 and the N-terminal eight residues remained invisible.

[1] This was confirmed by 1.4 Å resolution X-ray analysis of native ARP (pH 5.6) at 100 K; the Fe atom deviates from the pyrrole N plane by 0.32 Å towards the proximal His184 (unpublished result).

We thank Drs M. Kawamoto and H. Sakai (JASRI) for their help with data collection using synchrotron radiation at SPring-8 and Dr M. Sugishima for processing X-ray data. The synchrotron experiments were performed at BL41XU with the approval of JASRI (2001A0240-NL-np). This work was supported in part by a Grant-in-Aid for Scientific Research (C) (No. 14580674) and by a grant from the National Project on Protein Structural and Functional Analysis to KF from the Ministry of Education, Culture, Sports, Science and Technology of Japan.

References

Akimoto, K., Shinmen, Y., Sumida, M., Asami, S., Amachi, T., Yoshizumi, H., Saeki, Y., Shimizu, S. & Yamada, H. (1990). *Anal. Biochem.* **189**, 182–185.
Badyal, S. K., Joyce, M. G., Sharp, K. H., Seward, H. E., Mewies, M., Basran, J., Macdonald, I. K., Moody, P. C. & Raven, E. L. (2006). *J. Biol. Chem.* **281**, 24512–24520.
Brünger, A. T. (1992). *X-PLOR. A System for X-ray Crystallography and NMR.* Yale University, Connecticut, USA.
Chen, G. X. & Asada, K. (1989). *Plant Cell Physiol.* **30**, 987–998.
Collaborative Computational Project, Number 4 (1994). *Acta Cryst.* D**50**, 760–763.
Dauter, Z., Lamzin, V. S. & Wilson, K. S. (1997). *Curr. Opin. Struct. Biol.* **7**, 681–688.
DeLano, W. L. (2002). *The PyMOL Molecular Graphics System.* DeLano Scientific LLC, San Carlos, CA, USA.
Ermler, U., Grabarse, W., Shima, S., Goubeaud, M. & Thauer, R. K. (1997). *Science*, **278**, 1457–1462.
Finzel, B. C., Poulos, T. L. & Kraut, J. (1984). *J. Biol. Chem.* **259**, 13027–13036.
Fukuyama, K. (2001). *Handbook of Metalloproteins*, edited by A. Messerschmidt, R. Huber, T. Poulos & K. Wieghardt, pp. 222–232. Chichester: John Wiley & Sons.
Fukuyama, K., Kunishima, N., Amada, F., Kubota, T. & Matsubara, H. (1995). *J. Biol. Chem.* **270**, 21884–21892.

Gajhede, M. (2001). *Handbook of Metalloproteins*, edited by A. Messerschmidt, R. Huber, T. Poulos & K. Wieghardt, pp. 195–210. Chichester: John Wiley & Sons.
Gajhede, M., Schuller, D. J., Henriksen, A., Smith, A. T. & Poulos, T. L. (1997). *Nature Struct. Biol.* **4**, 1032–1038.
Henriksen, A., Smith, A. T. & Gajhede, M. (1999). *J. Biol. Chem.* **274**, 35005–35011.
Henriksen, A., Welinder, K. G. & Gajhede, M. (1998). *J. Biol. Chem.* **273**, 2241–2248.
Igarashi, N., Moriyama, H., Fujiwara, T., Fukumori, Y. & Tanaka, N. (1997). *Nature Struct. Biol.* **4**, 276–284.
Kunishima, N., Amada, F., Fukuyama, K., Kawamoto, M., Matsunaga, T. & Matsubara, H. (1996). *FEBS Lett.* **378**, 291–294.
Kunishima, N., Fukuyama, K., Matsubara, H., Hatanaka, H., Shibano, Y. & Amachi, T. (1994). *J. Mol. Biol.* **235**, 331–344.
Kunishima, N., Fukuyama, K., Wakabayashi, S., Sumida, M., Takaya, M., Shibano, Y., Amachi, T. & Matsubara, H. (1993). *Proteins*, **15**, 216–220.
Leslie, A. G. W. (1992). *Jnt CCP4/ESF–EACBM Newsl. Protein Crystallogr.* **26**.
Longhi, S., Czjzek, M. & Cambillau, C. (1998). *Curr. Opin. Struct. Biol.* **8**, 730–737.
Matsumoto, T., Nonaka, T., Hashimoto, M., Watanabe, T. & Mitsui, Y. (1999). *Proc. Jpn Acad.* **75**, 269–274.
Poulos, T. L., Edwards, S. L., Wariishi, H. & Gold, M. H. (1993). *J. Biol. Chem.* **268**, 4429–4440.
Ropp, J. S. de, La Mar, G. N., Wariishi, H. & Gold, M. H. (1991). *J. Biol. Chem.* **266**, 15001–15008.
Sawai-Hatanaka, H., Ashikari, T., Tanaka, Y., Asada, Y., Nakayama, T., Minakata, H., Kunishima, N., Fukuyama, K., Yamada, H., Shibano, Y. & Amachi, T. (1995). *Biosci. Biotechnol. Biochem.* **59**, 1221–1228.
Schuller, D. J., Ban, N., Huystee, R. B., McPherson, A. & Poulos, T. L. (1996). *Structure*, **4**, 311–321.
Sharp, K. H., Mewies, M., Moody, P. C. & Raven, E. L. (2003). *Nature Struct. Biol.* **10**, 303–307.
Sheldrick, G. M. & Schneider, T. R. (1997). *Methods Enzymol.* **277**, 319–343.
Shimizu, T., Nakatsu, T., Miyairi, K., Okuno, T. & Kato, H. (2002). *Biochemistry*, **41**, 6651–6659.
Shimizu, H., Park, S. Y., Shiro, Y. & Adachi, S. (2002). *Acta Cryst.* D**58**, 81–89.
Shinmen, Y., Asami, S., Amachi, T., Shimizu, S. & Yamada, H. (1986). *Agric. Biol. Chem.* **50**, 247–249.
Smith, A. T. & Veitch, N. C. (1998). *Curr. Opin. Chem. Biol.* **2**, 269–278.
Stec, B. & Phillips, G. N. Jr (2001). *Acta Cryst.* D**57**, 751–754.
Sugishima, M., Sakamoto, H., Higashimoto, Y., Omata, Y., Hayashi, S., Noguchi, M. & Fukuyama, K. (2002). *J. Biol. Chem.* **277**, 45086–45090.
Sugishima, M., Sakamoto, H., Noguchi, M. & Fukuyama, K. (2003). *Biochemistry*, **42**, 9898–9905.
Sundaramoorthy, M., Kishi, K., Gold, M. H. & Poulos, T. L. (1994). *J. Biol. Chem.* **269**, 32759–32767.
Tame, J. R. (2000). *Acta Cryst.* D**56**, 1554–1559.
Tame, J. R., Sleigh, S. H., Wilkinson, A. J. & Ladbury, J. E. (1996). *Nature Struct. Biol.* **3**, 998–1001.
Wariishi, H., Nonaka, D., Johjima, T., Nakamura, N., Naruta, Y., Kubo, S. & Fukuyama, K. (2000). *J. Biol. Chem.* **275**, 32919–32924.
Welinder, K. G. (1992). *Curr. Opin. Struct. Biol.* **2**, 388–393.